

Microstructural observations and tensile fracture behavior of FSW twin roll cast AZ31 Mg sheets

A. Dorbane^{a,e}, G. Ayoub^{a,b,*}, B. Mansoor^a, R.F. Hamade^b, G. Kridli^{a,c}, R. Shabadi^d, A. Imad^e

^a Department of Mechanical Engineering, Texas A&M University at Qatar, Doha, Qatar

^b Department of Mechanical Engineering, American University of Beirut, PO Box 11-0236, Beirut, Lebanon

^c Center for Lightweighting Automotive Materials and Processing, University of Michigan-Dearborn, Dearborn, MI, USA

^d Laboratory of Physical Metallurgy and Materials Engineering, UMET, UMR CNRS 8207, University of Lille 1 – Science and Technology, Villeneuve d'Ascq Cédex, France

^e Mechanics Laboratory of Lille, CNRS UMR 8107, Ecole Polytech'Lille, University of Lille 1 – Science and Technology, Villeneuve d'Ascq Cédex, France

ARTICLE INFO

Article history:

Received 26 July 2015

Received in revised form

19 September 2015

Accepted 24 September 2015

Available online 30 September 2015

Keywords:

Friction stir welding

Microstructure characterization

Mechanical response

Micro-hardness

Texture

Failure

ABSTRACT

Defect-free joints were friction stir welded (FSW) from AZ31 Mg alloy sheets by employing optimum welding parameters for the tool geometry used. Microstructure, texture and mechanical response of the welded joints were studied to identify susceptibility of crack initiation in the different weld zones and to understand the overall fracture behavior of these welds. Uniaxial tensile testing conducted orthogonal to the welding direction at temperatures of 25, 100, 200, and 300 °C revealed that cracks initiated mainly on the tool's advancing side (AS) of the weld between thermo-mechanically affected zone (TMAZ) and stir zone (SZ). Such cracks were found to propagate preferentially along this interfacial region leading to complete fracture. This finding may be linked to the inhomogeneous plastic deformation in the weld resulting in strong texture and microhardness gradients at the interface region between the TMAZ (AS) and the SZ. On the other hand, in tensile samples machined along the welding direction and containing stir zone microstructure, second phase particles were identified as the preferred sites for cracks initiation.

© 2015 Elsevier B.V. All rights reserved.

1. Introduction

Transportation industry has an increasing interest in replacing conventional alloys by lighter materials, due to its attractive specific mechanical properties magnesium alloys are the most adequate replacement [1,2]. Friction stir welding (FSW) is a promising joining method for magnesium alloys sheets. The reliability of structural parts joined by FSW is of high importance and, as such, investigating the microstructure, texture and mechanical properties of FSW joints is crucial to guide design engineers.

Friction stir welding (FSW) is a solid-state joining process, introduced in 1991 by the welding institute. FSW is carried out by inserting a rotating tool with a shoulder and pin between two metal sheets held together and translating it along the weld line. The rubbing action of the tool shoulder on metal surface generates frictional heat that increases the temperature to reach 70–80% of the material's melting temperature [3,4]. The frictional heating coupled with intense stirring and forging of the softened metal

due to rotating pin creates the FSW joint [5]. The microstructural and mechanical properties of welded joints are governed by the flow properties of the metal and the temperature distribution during welding. They are significantly dependent on the tool geometrical features and the choice of welding parameters e.g., rotation speed, feed rate, tilt angle and downward force [4,6–14].

FSW was originally developed in order to weld aluminum and its alloys, but recently it has been implemented to weld other materials such as copper and its alloys [15–18], steel and its alloys [19–21] and titanium and its alloys [22]. Also, several studies have reported welding or processing of magnesium and its alloys using friction stir welding technique. [23,24] reported that, with optimized welding parameters, the maximum tensile strength of the weld reached 93% that of the base material. [25,26] modified the structure of the magnesium alloys using friction stir processing and studied the microstructural, mechanical and texture properties and their evolution with different processing conditions. Recently, [27] related the average grain size obtained during friction stir processing of twin-roll-cast AZ31B magnesium alloy to the Zener–Hollomon parameter calculated using an experimentally verified finite element model. Although, the optimization of the welding parameters such as the tool rotation speed; tool travel speed is critical to obtain high quality welds, the optimization of

* Corresponding author at: Department of Mechanical Engineering, Texas A&M University at Qatar, Doha, Qatar.

E-mail address: georges.ayoub@qatar.tamu.edu (G. Ayoub).

the tool geometry and tool materials are also of high importance. [28] studied the effect of tool material, pin profile and diameter and shoulder diameter on the FSW weld quality of 6 mm thick AZ31B plates.

An extensive literature exists on the fracture behavior of FSW joints in Al alloys, however in comparison, magnesium alloys have received rather less attention. Several studies have reported that in FSW of AZ31 Mg the tensile property, particularly tensile elongation and UTS are significantly reduced which was mainly attributed to the variations in grain size, texture and nugget shape. A few studies on fracture behavior reported that when loading is applied perpendicular to the joint direction, depending on the FSW conditions, the fracture may occur in the heat affected zone (HAZ) or TMAZ either on the advancing side (AS) or retreating side (RS) of the weld [29–32]. The fracture behavior was mainly explained on the basis of through the thickness and length deformation and microstructural inhomogeneity in weld zones. Therefore, obtaining welds with a gradual grain size gradient between the different weld zones should be considered in the optimization schemes while selecting FSW parameters.

In this paper, we investigate the microstructure, texture, and mechanical response of friction stir welds of twin roll cast (TRC) AZ31B Mg sheets. We study their tensile fracture behavior to reveal the interplay between microstructural characteristics and propensity of crack initiation in different weld zones.

2. Experimental

2.1. Materials and welding

As a solid state joining process friction stir welding (FSW) results in highly characteristic asymmetric microstructure. The softened material, due to the rotating pin inducing frictional heat coupled with intense stirring and forging, reaches 70–80% of the material's melting temperature. Consequently, no solidification process from a melt is taking place. More or less, the final texture results from a rotation of the initial texture, which is highly dependent on the processing parameters. Therefore, a continuous evolution of the texture and microstructure is obtained throughout the different weld zone preserving higher weld integrity. The FSW setup was mounted on a HAAS VF6 vertical machining center (for experimental details see [33]). A backing plate and two holders, both made from C30 steel constituted the fixture to firmly hold the workpiece. The FSW tool was machined from SVERKER 21 (i.e., AISI-D2) tool steel supplied by Uddeholms AB (SE-683 85 Hagfors, Sweden). The tool was hardened after machining. The cylindrical tool has a shoulder diameter of 19 mm, and a pin of 6.4 mm in diameter with a pin length of 2.7 mm. Both the pin and the shoulder of the tool have smooth cylindrical shapes. All the welds, studied in this paper, were achieved using 1200 rpm tool rotation speed and 150 mm/min welding speed. These chosen process parameters yielded maximum strength (as reported by previous work of some of the authors [34]).

The plates welded in this study were twin roll cast (TRC) AZ31B magnesium alloy rolled to a final thickness of 3 mm and supplied by POSCO. In all welds, welding was carried out along the rolling direction of the AZ31B sheets. The nominal chemical composition of this alloy is shown in Table 1.

Table 1
Nominal chemical composition of AZ31B.

Component	Mg	Al	Zn	Mn	Si
Amount (wt%)	95.43	3.32	0.80	0.30	0.15

2.2. Microstructure and texture

To analyze the microstructure, the standard metallographic preparation method was used to prepare the samples, following the E3 ASTM standards [35]. Etching was performed using an acetic picral solution composed of 4.2 g picric acid, 10 ml acetic acid, 70 ml ethanol and 10 ml water. Micrographs were taken using “Zeiss Axiovert 40 MAT” optical light microscope. The grain size analysis was performed using AxioVision software with a grain size analyzer module.

Microstructural and textural analyses of the welds obtained by FSW of AZ31B sheets were performed using electron backscatter diffraction (EBSD). Specimens were cut from the different zones of the weld and oriented for observation in the TD–ND plane (refer to the Section 3). The samples were prepared using a standard preparation method for EBSD. The EBSD analyses were performed on a FEI Field Emission Scanning Microscope (FESEM). All scans were conducted using an accelerating voltage of 20 KeV and a probe current of ~ 10 nA. The TSL Orientation Imaging Microscopy (OIM) Analysis EBSD software was used to analyze the micrographs. A filter was used to eliminate any data with a confidence index (CI) below 0.1.

2.3. Mechanical properties

Mechanical properties of welds were characterized using Vickers hardness testing, with 100 g force for a dwell time of 15 s on the samples cut in the transverse direction to the weld. Uniaxial tensile tests were performed at 25 °C, 100 °C, 200 °C and 300 °C under constant strain rate of 10^{-3} s^{-1} using an MTS Insight electromechanical testing machine with a 30 kN load cell equipped with a LBO-series Thermcraft LabTemp (Environmental chamber). Tensile test samples were cut from the stir zone (SZ) to characterize purely the SZ behavior. Another set of samples was cut with the major axis being perpendicular to the welding direction, to study the influence of overall microstructural change caused by the friction stir tool movement on the mechanical properties. Samples from the SZ region and the ones taken perpendicular to the welding region are referred to in the manuscript as the FSW parallel direction and FSW perpendicular direction, respectively.

3. Microstructural observations and textural analysis

Fig. 1(a) shows a schematic illustration of the FSW process, the labeling of the three directions of the sheet are indicated; corresponding to the welding direction (WD), transverse direction (TD) and normal direction (ND). Fig. 1(b) shows the overall structure of the friction stir welded joint cross-section (ND–TD plane). The contours of the different zones constituting the cross-sectional macrostructure were highlighted on the Fig. 1(b). Four distinguishable areas can be observed, such as the base metal (BM), heat affected zone (HAZ), thermo-mechanically affected zone (TMAZ) and the stir zone (SZ). Similar observations of the weld zones and shape of the nugget were reported by several studies on different alloys [12,36–38].

A cross section along a friction stir welded AZ31B joint is shown in Fig. 2 which shows the microstructure of the different weld zones identified in Fig. 1. The four weld zones clearly exhibit distinguishable microstructure. While the base metal contains mainly an equiaxed grain structure, the heat-affected zone may be characterized as a bimodal grain structure with the presence of a fair number of what appears to be twins (as the AZ31B base metal was deformed by rolling). The thermo-mechanically affected zone shows elongated grains with the presence of a larger number of

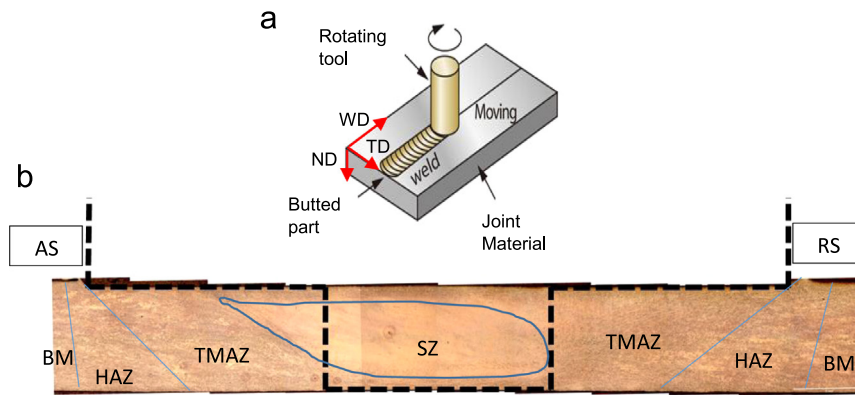


Fig. 1. (a) Schematic illustration of FSW process. (b) Microstructure of TRC AZ31B sheets welded by FSW with parameters of 1200 rpm and 150 mm/min.

twins. The stir zone contains mainly a homogeneous distribution of the grains. The average grain size of the different weld zones were found to be equal to $8.17\ \mu\text{m}$ for the base metal, $10.45\ \mu\text{m}$ for the heat affected zone, $11.47\ \mu\text{m}$ for the thermo-mechanically affected zone and $12.13\ \mu\text{m}$ for the stir zone. These observations are in line with observations of the microstructure of friction stir welded AZ31B reported by [23,25,39].

EBSD scans from three weld zones, SZ, TMAZ advancing side (AS) and TMAZ retreating side (RS) are shown in Fig. 3. The grain size as well as the grains orientation on a larger number of grains can be extracted from this figure. The microstructure observed in the EBSD scans are in coherence with the optical microscope observations; such as homogeneous distribution of the grains in the SZ and elongated grains with a larger number of twins in the TMAZ. The EBSD software revealed a grain size of $18.8\ \mu\text{m}$ for the SZ, $7.8\ \mu\text{m}$ for the TMAZ (AS) and $8\ \mu\text{m}$ for the TMAZ (RS). The difference in the grain size between the OM micrographs and EBSD micrographs is likely due to the different grain size calculation methods used. From the EBSD scans, the grain orientations of the three different weld zones was represented through pole

figures in the (0002) and (1010) planes, as shown in Fig. 4. The as-received material has a typical rolled texture with the c axis of the grains perpendicular to the TD–RD plane (see [40,26]). Fig. 4 (a) shows the texture of the TMAZ and HAZ in the advancing side. The (0002) pole figure reveals a texture strengthening with one basal peak that appears shifted from the left end of the ND axis. However the (1010) pole figure shows a random orientation of the six prismatic planes. Fig. 4(b) shows the texture of the nugget zone (stir zone). Two basal peaks appear along the ND axis shifted from the ends in the (0002) pole figure. The strengthening of the texture is most probably due to the rotation of the c -axis around the transverse direction (TD). The (1010) pole figure shows a number of intensity peaks along the TD resulting of the lattice rotation. Finally Fig. 4(c) shows the texture of TMAZ and HAZ in the retreating side. The figure shows a high strengthening of the basal texture with the initial c -axis being rotated of about 10° counter clock wise around WD.

As general observation, the SZ encountered severe deformation and the microstructural and textural analysis showed a recrystallized microstructure with strengthening of the basal

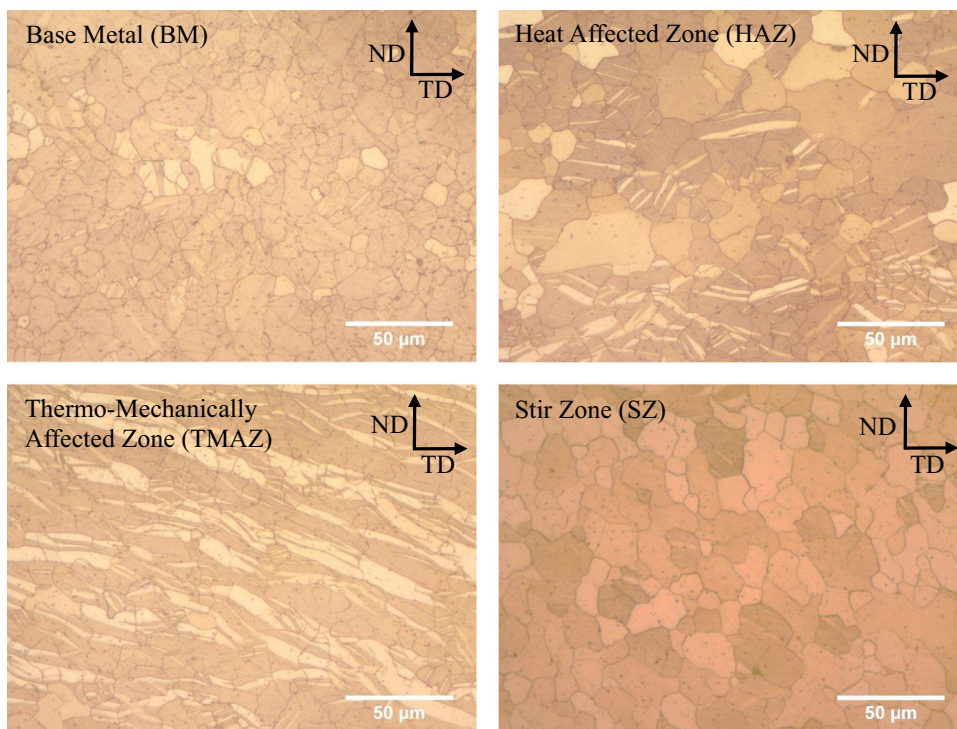


Fig. 2. Microstructure of the zones observed in the welded joint using parameters of 1200 rpm and 150 mm/min.

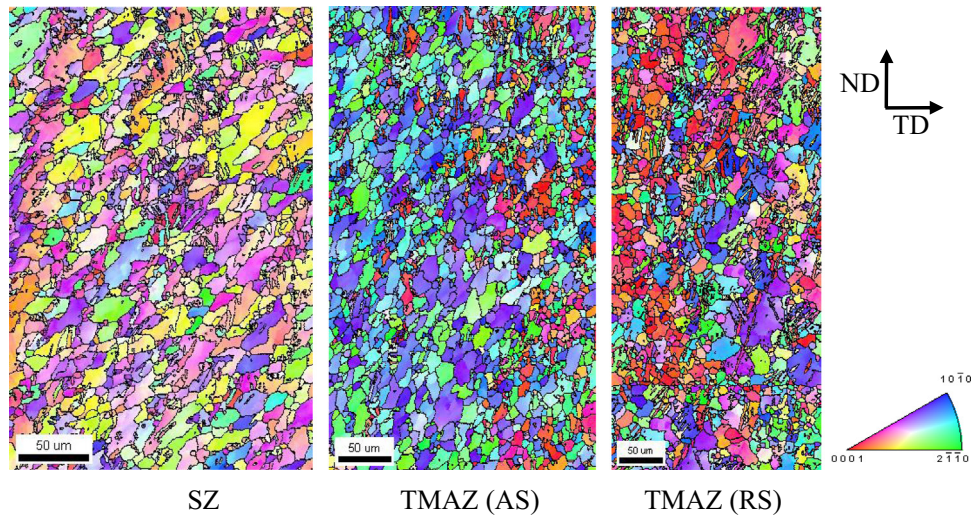


Fig. 3. EBSD scans of the three different weld zones, SZ, TMAZ in the advancing side (AS) and TMAZ in the retreating side (RS).

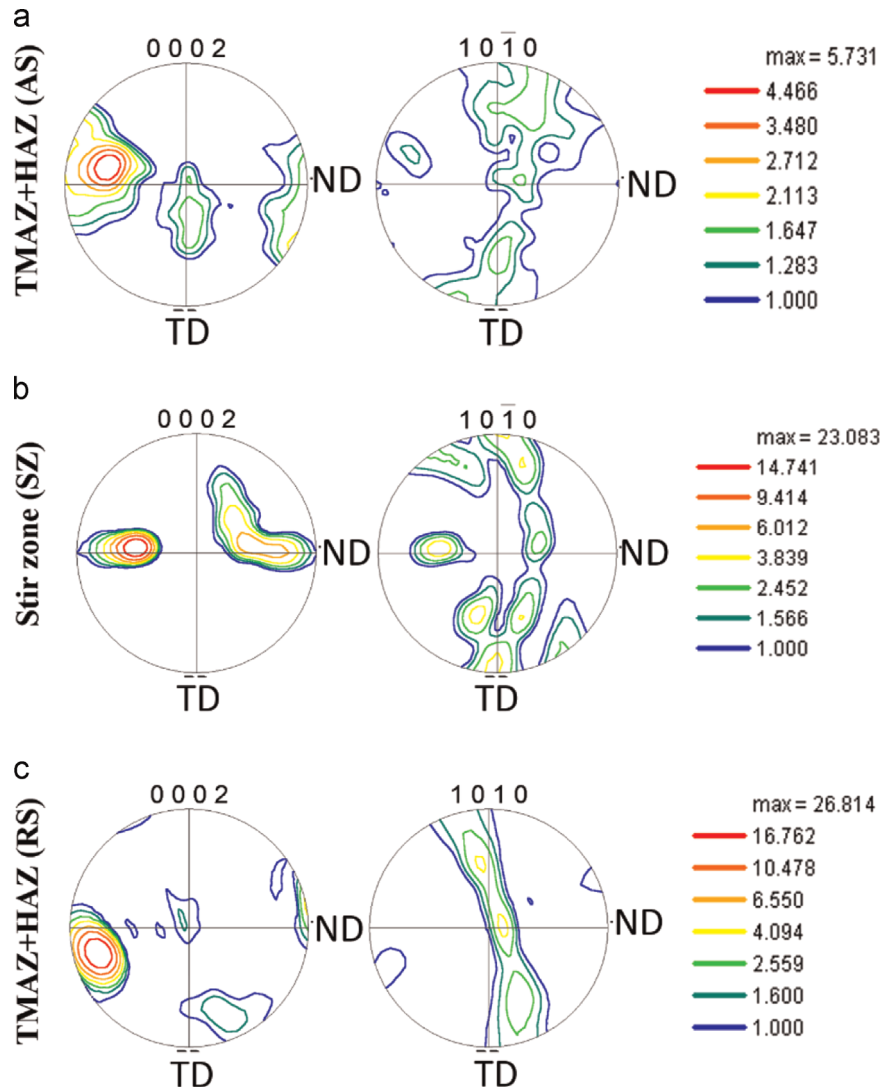


Fig. 4. Pole figures representing the texture for different samples, (a) TMAZ+HAZ on the advancing side; (b) Stir zone (SZ) and (c) TMAZ+HAZ on the retreating side (RS).

texture. The microstructural and textural analysis of the TMAZ (AS) pointed to a low level of deformation as slight modification of the microstructure and texture compared to the base metal was

observed. A higher level of deformation appears to have taken place in the TMAZ (RS) as compared to the TMAZ (AS) (but lower level of deformation has occurred as compared with the SZ with

strengthening of the basal texture).

4. Micro-hardness testing

In order to identify the zones in the weld where the fracture is more likely to occur, vickers microhardness tests were performed along the TD on the TD–ND plane of the TRC friction stir welded sheets. The results are shown plotted in Fig. 5. The distance between two indentation points was 0.25 mm. The analysis was performed on three lines across the thickness of the sheet and parallel to TD as shown in Fig. 5, the distance between each line is 0.5 mm. The measured hardness values were found to vary between a low of 55 and high of 85 HV. This variation is perhaps due to the evolution of the grain size along the TD in the joint as pointed out in Section 3. The center of the joint exhibited the least micro-hardness values compared to the other zones, which can be explained by the fact that the grains are equiaxed and also the occurrence of recrystallization and recovery in the stir zone. Similar observations were reported by [41] and [42] who reported that in addition to grain size evolution the dissolution of the precipitates due to frictional heating is one of the main causes of the decrease in the hardness and yield strength values. To highlight the relation between grain size and micro-hardness values, Fig. 6 plots the reciprocal of the square root of the average grain size ($d^{-1/2}$) as function of the micro-hardness obtained along TD of the weld cross-section. Average hardness values taken from the SZ, TMAZ, HAZ and BM were plotted as a function of the average grain sizes. It can be highlighted that the Vickers hardness values are strongly dependent on the grain size. A linear relation was found and is agreement with the Hall–Petch relationship. Similar trend were reported by [23] who reported that smaller the grain sizes large is the grain boundary surface that offers more difficulty for the deformation to occur, hence the higher hardness.

The vickers microhardness tests show a continuity in the hardness values at the interface between the SZ and the TMAZ (RS), however a peak of the hardness values was measured at the interface between the SZ and the TMAZ (AS). The discontinuity of the hardness values between the SZ and the TMAZ (AS) can be related to an abrupt change in the microstructure, more precisely the grain size and also an abrupt change in the texture (as reported previously in Section 3). Actually, the material in the advancing

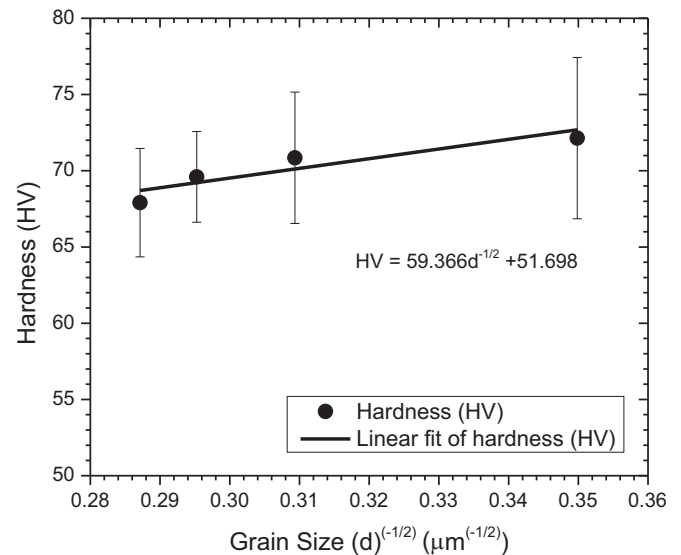


Fig. 6. Relationship between the grain size and micro-hardness.

side of the tool is relatively cooler than on the retreating side, hence, larger deformation is induced in the retreating side. Therefore, we assume that a higher level of incoherency at the interface between the SZ and the TMAZ (AS) will induce higher accumulation of dislocations. This higher density of dislocations further hastens the process of crack initiation when the weld is under tensile loading conditions.

5. Uniaxial tensile testing and fracture initiation

The quality of the weld can be verified by characterizing the mechanical properties under tensile testing at different temperatures to account for potential ranges in service conditions. Therefore, the FSW parallel and perpendicular direction samples were tested between room temperature to 300 °C. It is worth pointing out that the FSW tool pin diameter was equal to 6.4 mm and the sample gauge width is 6 mm, therefore the FSW parallel direction samples represent the stir zone behavior under uniaxial loading. The geometry of the tensile test samples was selected according to E8 ASTM standards [43] is shown in Fig. 7. The tensile test samples were mechanically polished to eliminate the marks left on the surface by the FSW process or by the subsequent machining. The joint strength was measured for both types of samples. In the purpose of verifying the repeatability of the results each tested condition was repeated at least two times.

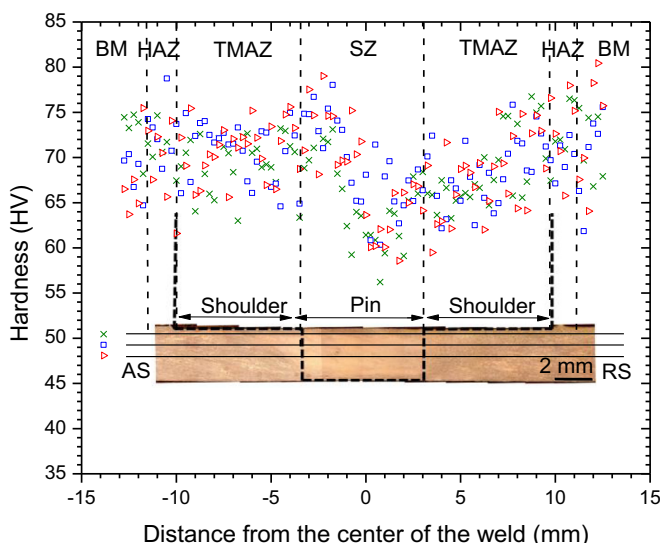


Fig. 5. Microhardness measurements at the cross section of the weld.

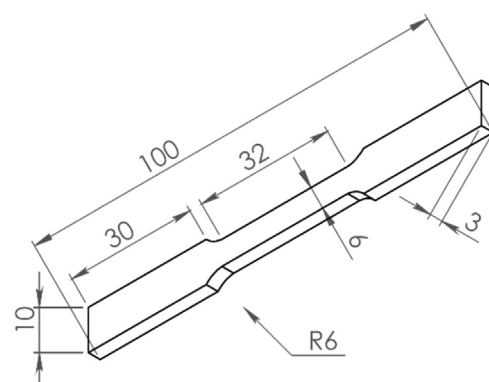


Fig. 7. Uniaxial tensile testing geometry (ASTM E8/E08M) (dimensions are in mm).

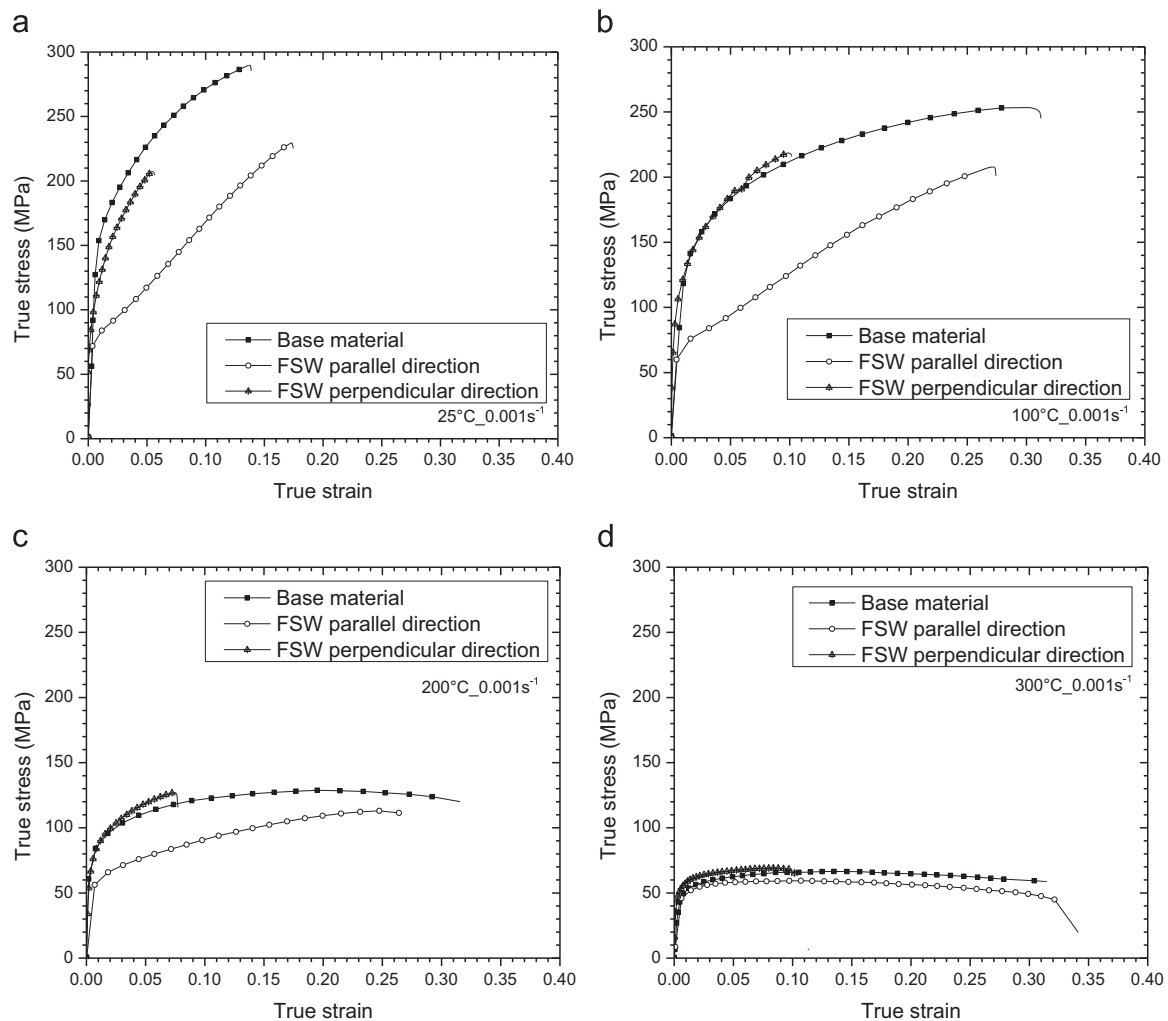


Fig. 8. True stress-true strain curves of uniaxial tensile testing of AZ31B base material, FS welded tested in the parallel direction, and perpendicular direction under strain rate of 10^{-3} s^{-1} (a) 25 °C, (b) 100 °C, (c) 200 °C and (d) 300 °C.

Fig. 8 shows the uniaxial true stress–strain curves of the base metal,¹ the FSW perpendicular direction and FSW parallel direction samples tested at different temperatures. Overall, it was observed that the base material exhibit higher yield stress and ultimate tensile strength than the FSW perpendicular and parallel samples. As a general observation, the FSW perpendicular samples exhibit higher ultimate tensile strength than the FSW parallel samples, Fig. 8. This trend was expected as the FSW parallel samples were cut from the stir zone, which has the largest average grain size. The grain boundaries act as dislocation barriers during deformation, the SZ has less grain boundaries since it exhibited equiaxed grains and the largest grain size. Therefore, we expect that the SZ would exhibit the lowest yield stress and ultimate tensile strength and the highest elongation to fracture as evidenced by the tensile test curves for all the tested temperatures. These results are in agreement with the microstructure and microhardness data presented in Section 4. Fig. 8 shows that the FSW perpendicular samples encountered the lowest strain to fracture. Principally, the fracture in the FSW perpendicular samples occurred between the stir zone and the thermo-mechanically affected zone in the advancing side. The interfacial region between

the SZ and the TMAZ (AS) is characterized by a higher degree of incoherency as an abrupt change of the texture is reported in Section 3 and also the highest hardness values represented in Fig. 5. The interface region between the SZ and TMAZ (AS) proves to be a weak region where the cracks are most probable to initiate, which may explains the lowest UTS and strain to fracture exhibited by the FSW perpendicular samples.

It is observed that, with increasing temperature, for all samples, a decrease in the yield stress and ultimate tensile strength and an increase of the strain to fracture are the characteristics of the tensile test curves. It is due to the fact that the work hardening capacity of the material decreases with increasing temperature. Work softening was not observed at RT for all samples but at 100 °C the base metal showed some softening, however the welded samples didn't show any softening as they fractured after reaching the ultimate tensile strength. At 200 °C, it was observed that the base material shows work hardening and work softening during deformation and the welded material experienced work hardening and slight work softening before fracture. At 300 °C, the work to softening was predominant in the deformation process before the fracture for the base material and both welded specimens.

The evolution of the mechanical properties and more precisely the yield stress, ultimate tensile strength, the strain to fracture for the different samples and the Ramberg–Osgood hardening and plastic flow resistance coefficients (base material, FSW parallel and

¹ The stress was calculated $\sigma = F/A$ with F being the measured load and A the current cross-sectional area. A was calculated by assuming that the material deforms at a constant volume although this assumption doesn't hold true after necking.

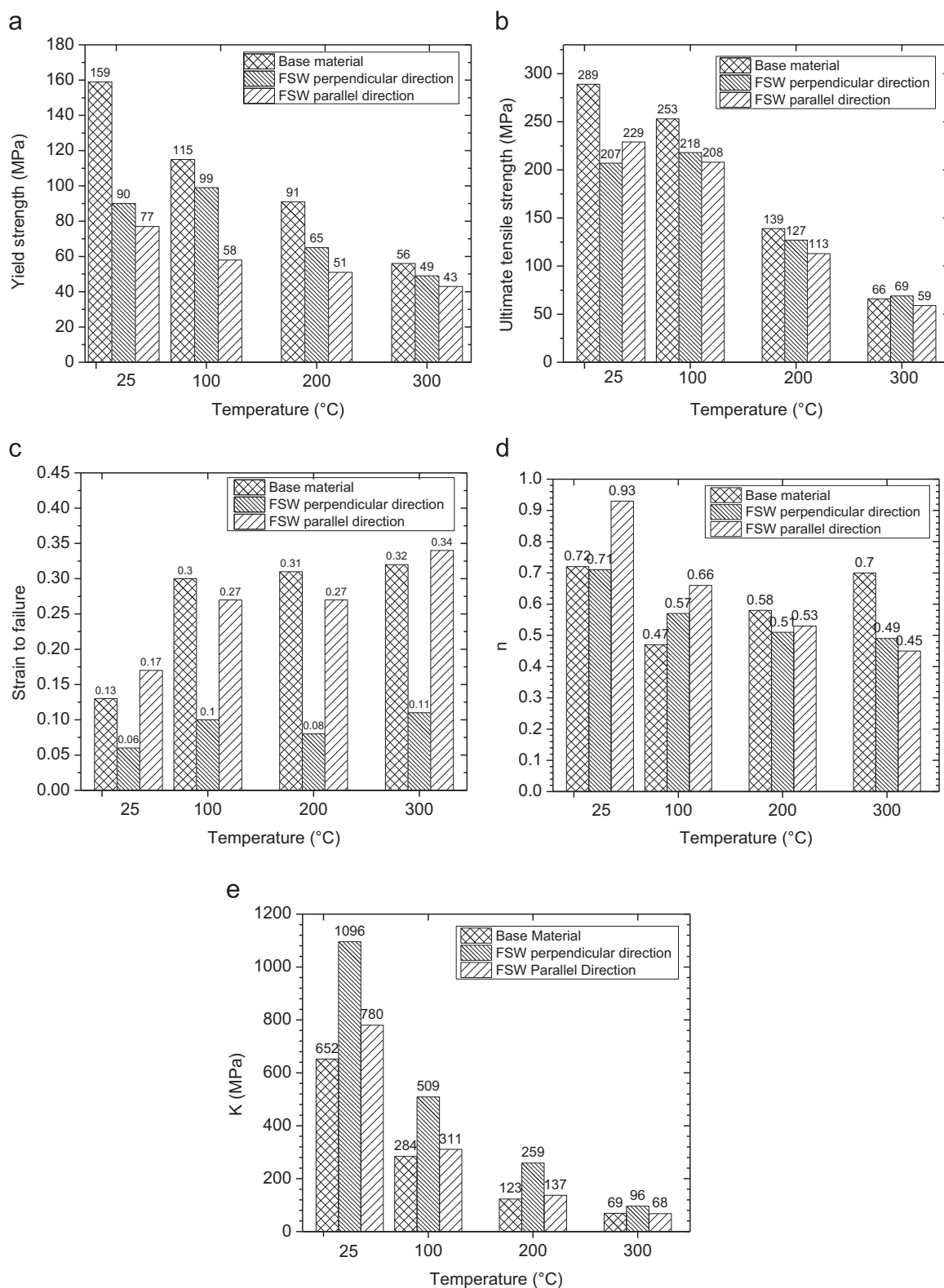


Fig. 9. (a) Ultimate tensile strength, (b) yield strength, (c) strain to failure, (d) strain hardening, (e) plastic flow of the base material and FSW specimens in the perpendicular and parallel directions, at different temperatures and constant strain rate of 10^{-3} s^{-1} .

FSW perpendicular samples) tested at four different temperatures are summarized in Fig. 9. Fig. 9(a) shows that the yield stress gradually decreased with increasing temperature for the three tested samples; from 159 MPa to 56 MPa for the base metal, from 90 MPa to 49 MPa for the FSW perpendicular samples and finally from 77 MPa to 43 MPa for the FSW parallel samples. As was

pointed out previously, the yield stress of the FSW perpendicular samples is higher than yield stress of the FSW parallel direction. The ultimate tensile strength comparison of both base material and FSW samples in Fig. 9(b) showed a significant decrease with increasing temperature; from 289 MPa to 66 MPa for the base metal, from 207 MPa to 69 MPa for the FSW perpendicular

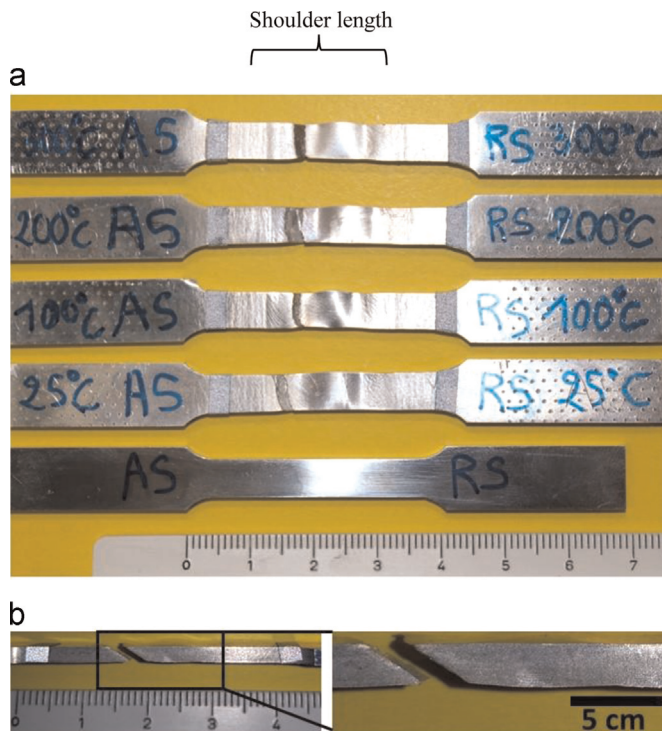


Fig.10. (a) Fractured samples at different temperatures. (b) Fractured sample showing the angle of the crack propagation.

samples and finally from 229 MPa to 59 MPa for the FSW parallel samples. The strain to fracture, Fig. 9(c), showed a significant increase in its values from 25 °C to 300 °C, 160% for the base metal, 83% for the FSW perpendicular samples and finally 100% for the FSW parallel samples. The FSW parallel samples showed higher ductility than the base material at room temperature and 300 °C and slightly inferior values at 100 °C and 200 °C. The FSW perpendicular samples showed the lowest strain to fracture with a fracture occurring between the TMAZ (AS) and the SZ.

The variations in the mechanical properties during the plastic regime were studied using the Ramberg–Osgood macroscopic model:

$$\sigma = \sigma_y + K\epsilon_p^n \quad (1)$$

where σ is the stress, σ_y is the yield stress, ϵ_p is the plastic strain, K is the plastic flow resistance coefficient and n is the strain hardening exponent. The K and n referred to as the Ramberg–Osgood coefficients were obtained by linear regression, by writing Eq. (1) in logarithmic formulation.

Fig. 9(d) shows an overall decrease in strain hardening with increasing temperature. The FSW parallel samples exhibited the highest strain hardening at RT and 100 °C, however the base metal showed the highest strain hardening at higher temperatures. Fig. 9 (e) shows the effect of temperature on the plastic flow resistance coefficient. As a general trend, it is observed that the values of the coefficient K increase with increasing temperature and the highest values were found for the FSW perpendicular samples, while the lowest values were found for the base material. A gradual change

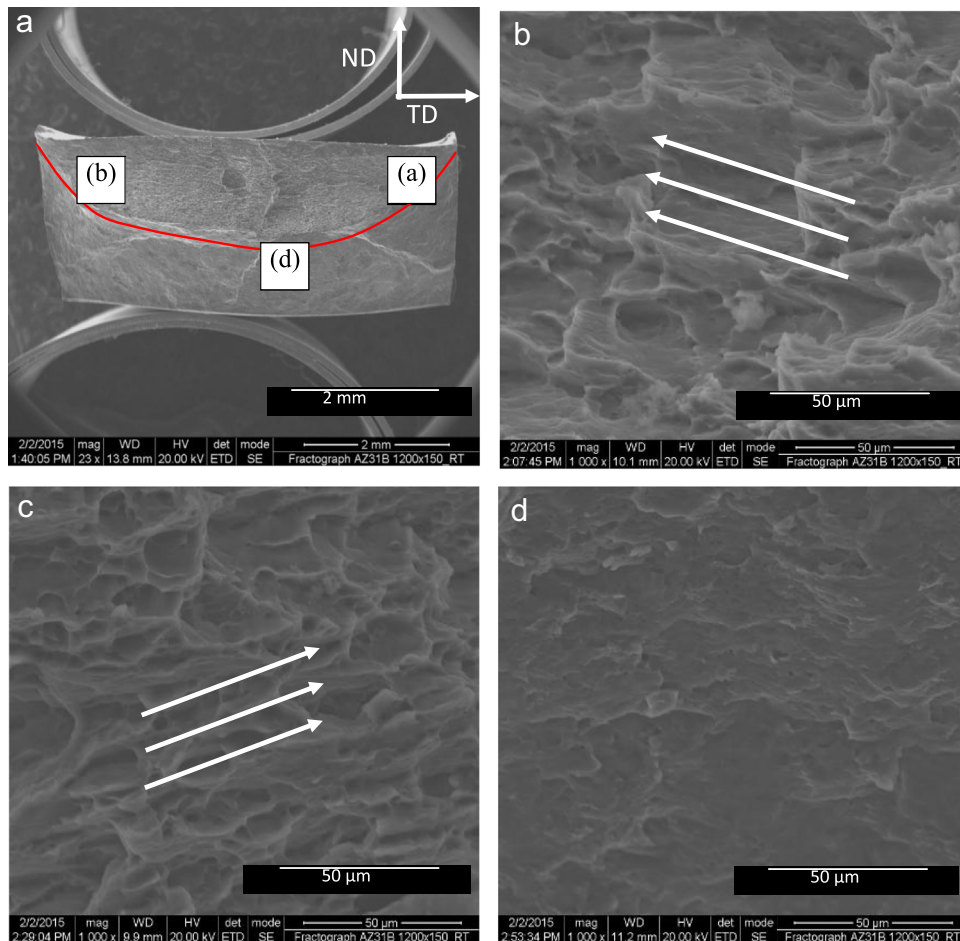


Fig. 11. Scanning Electron Microscope fractography of specimen deformed in the welding direction. (a) Low magnification. (b)–(d) Magnified regions. (For interpretation of the references to color in this figure, the reader is referred to the web version of this article.)

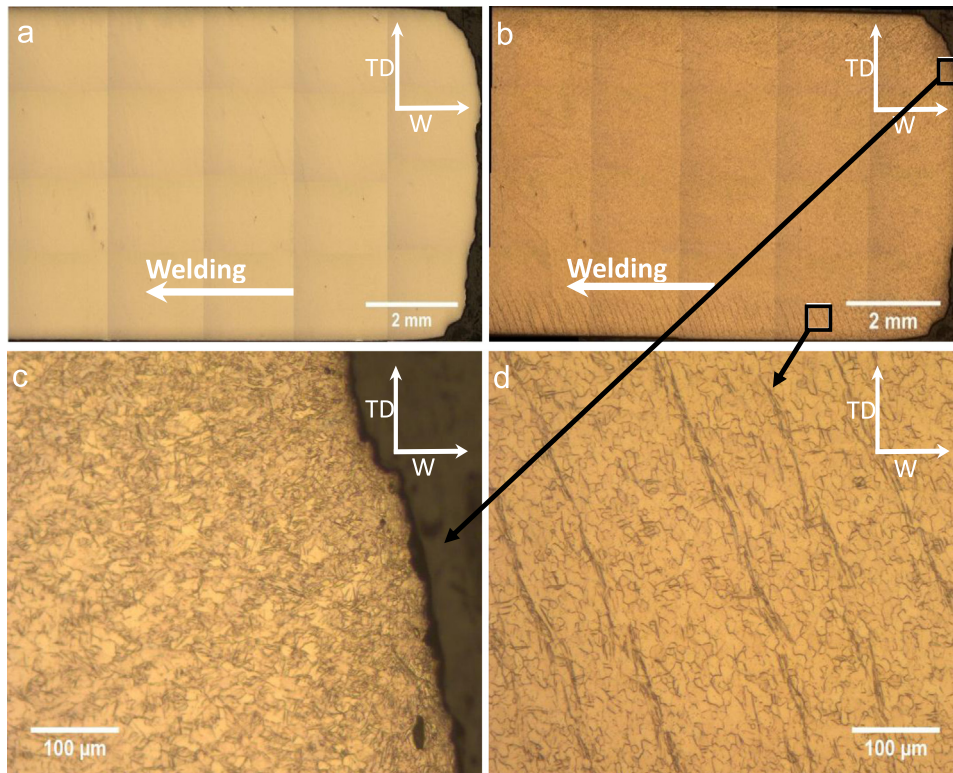


Fig. 12. Microstructure of fractured tensile test sample after tensile testing at 25 °C.

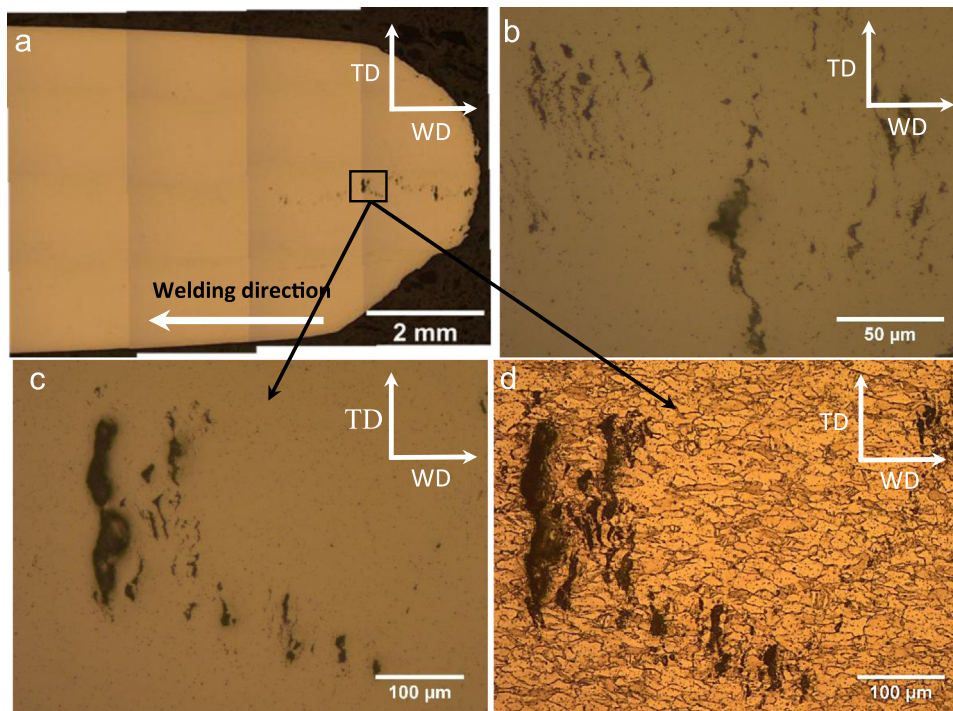


Fig. 13. Microstructure of fractured tensile test sample after tensile testing at 200 °C.

in the coefficient K was noticed; from 652 MPa to 69 MPa for the base metal, from 1096 MPa to 96 MPa for the FSW perpendicular samples, and finally from 780 MPa to 68 MPa for the FSW parallel samples. It is worth noticing that the samples taken from relatively homogeneous materials (base metal and FSW parallel samples)

exhibit similar values of coefficient K . However, much higher values are obtained for coefficient K with the FSW perpendicular samples, which may indicate the presence of high density of dislocation accumulation that translates by a higher hardening. Again, this observation is in coherence with our findings in

Sections 3 and 4, more precisely; the presence of higher amount of accumulated deformation/dislocations in the interfaces between SZ and TMAZ (AS).

Fig. 10 shows pictures of the FSW perpendicular samples after fracture under tensile test at temperatures of 25 °C, 100 °C, 200 °C and 300 °C. It is clearly shown that the fracture occurred between the SZ and the TMAZ in the advancing side with a slanted crack forming approximately at an angle of 45° (measured along the side of the sample, in the thickness) with the major axis of the sample (Fig. 10 (b)). Fig. 1 also shows that the interface region between the SZ and the TMAZ (AS) forms approximately an angle of 45° with the transverse direction. Therefore the crack was supposed to have propagated along this SZ and the TMAZ (AS) interface. This is in line with results reported by [23] and [44] who investigated the behavior of FS welded AZ31B. It can be concluded that the zone where cracks are the most probable to initiate in the friction stir welded AZ31 sheets is the interface line between SZ and the TMAZ (AS). Therefore the FSW process parameters should be optimized to improve the microstructural gradient between the SZ and the TMAZ (AS) interface.

6. Fractography analysis and damage mechanism in the stir zone

To investigate the damage mechanisms in the stir zone the fracture surface of the FSW parallel samples were observed with SEM. Fig. 11 shows a SEM micrographs of the fracture surface of FSW parallel samples tested at room temperature. Fig. 11(a) shows the fracture surface with low magnification, a typical ductile fracture surface is observed; a crack propagation zone above the red curved line and a brittle fracture surface below the line. Three different area of this heterogeneous morphology is observed with higher magnification. Fig. 11(b) shows the microstructure of the upper left region where the microscopic dimples direction is toward to left side. Fig. 11(c) shows the microstructure of the cross-section upper right side, it can be seen that the microscopic dimples are toward the right side. Finally, Fig. 11(d) shows the microstructure of the lower region where almost no dimples are observed. From those observations, it can be concluded that the crack initiated at the surface in the middle of the upper area of the sample and propagated in a shape of an arc of circles (as shown by the red curved line) until the samples couldn't withstand the load leading to a brittle fracture.

Furthermore, in order to study the crack initiation mechanisms in the stir zone, specimens from different planes were cut from the FSW parallel samples that were tested at different temperature. The specimens were polished then observed under an optical microscope. Fig. 12 shows an optical microscope mapping of the WD–TD plane of the failed sample previously deformed at room temperature. A low number of microcracks, mostly concentrated near the fracture surface, was observed explaining the lower ductility of the samples at RT. Fig. 12(c) shows bands of recrystallized grains parallel to each other in a zone free of cracks.

Moreover, the WD–TD plane of a failed sample deformed at 200 °C was observed with an optical microscope, the micrographs are shown in Fig. 13. The FSW parallel samples deformed at 200 °C exhibited work softening hence we assume that observation of microcracks is easier than at RT. Actually, as showed by Fig. 13 the micrographs contained many cracks compared to RT condition. The cracks propagated in a zigzag shape, however overall the cracks seems propagating perpendicularly to the loading direction.

[45] Studied the damage mechanisms in AZ31 at RT and reported that the majority of cracks initiate at the second phase particles and deformation twin. From Figs. 12 and 13(d) we assume that that the majority of cracks initiated in the second face

particles as no cracks initiating at the deformation twins were observed.

7. Conclusions

In order to study the mechanical, microstructural and textural properties of FSW joints; 3 mm thick AZ31B sheets were welded using optimum FSW welding conditions (found for a particular tool geometry used at spindle speed and tool feed rate of 1200 rpm and 150 mm/min, respectively).

As general observation of the microstructure and the texture: (a) the SZ exhibited a recrystallized microstructure characterized by minor grain growth and strengthening of the basal texture due to a rotation of the crystal *c*-axis around the WD; (b) the TMAZ on the AS presented a slight modification of the microstructure and texture compared to the base metal; (c) the TMAZ on the RS showed higher level of deformation compared to its counterpart but lower than the SZ, some recrystallization and some strengthening of the basal texture was also observed.

Vickers micro-hardness values measured were maximum at the interface between the SZ and the TMAZ in the AS and were attributed to an accumulated deformation that possibly induced a higher density of dislocations and abrupt change in the microtexture at the interface of TMAZ and SZ in the AS. Consequently, it was assumed that cracks would initiate at this interface between the SZ and the TMAZ in the AS due to a higher level of incoherency.

Uniaxial tensile testing conducted at strain rate of 10^{-3} s^{-1} and at different temperatures (25 °C, 100 °C, 200 °C, and 300 °C) revealed, a temperature dependent mechanical response. Specimens machined with their major axis parallel and perpendicular to the weld joint were tested and the results were compared to the mechanical behavior of the base metal. FSW perpendicular direction samples exhibited higher strength levels. The highest tensile elongation was exhibited by the FSW parallel samples. However, the lowest strain to fracture was achieved by the FSW perpendicular samples that presented a fracture occurring between the TMAZ and the SZ in the AS.

Failure mechanisms in the stir zone was investigated and a larger number of cracks were observed in the FSW (parallel samples) tested in tension at 200 °C compared to samples tested at RT. It was observed that the majority of cracks had initiated in the second-phase particles.

Acknowledgment

This work was made possible by NPRP Grant #4-1063-2-397 from Qatar National Research fund, Qatar (A member of Qatar Foundation). The statements made herein are solely the responsibility of the authors.

References

- [1] H. Friedrich, S. Schumann, J. Mater. Process. Technol. 117 (2001) 276–281.
- [2] A. Tharumarajah, P. Koltun, J. Clean. Prod. 15 (2007) 1007–1013.
- [3] K.A.A. Hassan, P.B. Prangnell, A.F. Norman, D.A. Price, S.W. Williams, Sci. Technol. Weld. Join. 8 (2003) 257–268.
- [4] W. Lee, K.-H. Chung, D. Kim, J. Kim, C. Kim, K. Okamoto, R.H. Wagoner, K. Chung, Int. J. Plast. 25 (2009) 1626–1654.
- [5] W.F. Xu, J.H. Liu, D.L. Chen, J. Alloy. Compd. 509 (2011) 8449–8454.
- [6] G. Buffa, J. Hua, R. Shivpuri, L. Fratini, Mater. Sci. Eng. A 419 (2006) 381–388.
- [7] R.S. Coelho, A. Kostka, S. Sheikhi, J. dos Santos, A.R. Pyzalla, Adv. Eng. Mater. 10 (2008) 961–972.
- [8] G.R. Cui, Z.Y. Ma, S.X. Li, Scr. Mater. 58 (2008) 1082–1085.
- [9] R.M. Leal, C. Leitão, A. Loureiro, D.M. Rodrigues, P. Vilaça, Mater. Sci. Eng. A 498

- (2015) 384–391.
- [10] W. Pan, D. Li, A.M. Tartakovsky, S. Ahzi, M. Khraisheh, M. Khaleel, *Int. J. Plast.* 48 (2013) 189–204.
- [11] A.L. Etter, T. Baudin, N. Fredj, R. Penelle, *Mater. Sci. Eng. A* 445–446 (2007) 94–99.
- [12] M. Peel, A. Steuwer, M. Preuss, P.J. Withers, *Acta Mater.* 51 (2003) 4791–4801.
- [13] J.Q. Su, T.W. Nelson, R. Mishra, M. Mahoney, *Acta Mater.* 51 (2003) 713–729.
- [14] W.M. Thomas, E.D. Nicholas, J.C. Needham, M.G. Murch, P. Temple-Smith, C.J. Dawes, GB patent no. 9125978.8, International Patent No. PCT/GB92/02203, 1991.
- [15] Y.M. Hwang, P.L. Fan, C.H. Lin, J. Mater. Process. Technol. 210 (2010) 1667–1672.
- [16] W.-B. Lee, S.-B. Jung, *Mater. Lett.* 58 (2004) 1041–1046.
- [17] T. Sakthivel, J. Mukhopadhyay, *JMatS* 42 (2007) 8126–8129.
- [18] K. Savolainen, T. Saukkonen, H. Hänninen, *Sci. Technol. Weld. Join.* 17 (2012) 111–115.
- [19] M. Matsushita, Y. Kitani, R. Ikeda, M. Ono, H. Fujii, Y.D. Chung, *Sci. Technol. Weld. Join.* 16 (2011) 181–187.
- [20] U.U. Ofem, P.A. Colegrove, A. Addison, M.J. Russell, *Sci. Technol. Weld. Join.* 15 (2010) 479–485.
- [21] S.H.C. Park, Y.S. Sato, H. Kokawa, K. Okamoto, S. Hirano, M. Inagaki, *Scr. Mater.* 49 (2003) 1175–1180.
- [22] Y. Zhang, Y.S. Sato, H. Kokawa, S.H.C. Park, S. Hirano, *Sci. Technol. Weld. Join.* 15 (2010) 500–505.
- [23] N. Afrin, D.L. Chen, X. Cao, M. Jahazi, *Mater. Sci. Eng. A* 472 (2008) 179–186.
- [24] W. Xunhong, W. Kuaishhe, *Mater. Sci. Eng. A* 431 (2006) 114–117.
- [25] B. Mansoor, A.K. Ghosh, *Acta Mater.* 60 (2012) 5079–5088.
- [26] J.P. Young, H. Askari, Y. Hovanski, M.J. Heiden, D.P. Field, *Mater. Charact.* 101 (2015) 9–19.
- [27] A.H. Ammouri, G. Kridli, G. Ayoub, R.F. Hamade, J. Mater. Process. Technol. 222 (2015) 301–306.
- [28] G. Padmanaban, V. Balasubramanian, *Mater. Des.* 30 (2009) 2647–2656.
- [29] D. Li, X. Yang, L. Cui, F. He, H. Shen, *Mater. Des.* 64 (2014) 251–260.
- [30] Y. Tao, Z. Zhang, D.R. Ni, D. Wang, B.L. Xiao, Z.Y. Ma, *Mater. Sci. Eng. A* 612 (2014) 236–245.
- [31] L. Wan, Y. Huang, W. Guo, S. Lv, J. Feng, J. Mater. Sci. Technol. 30 (2014) 1243–1250.
- [32] S.A. Khodir, Y. Morisada, R. Ueji, H. Fujii, *Mater. Sci. Eng. A* 558 (2012) 572–578.
- [33] A.H. Kheireddine, A.H. Ammouri, G.T. Kridli, R.F. Hamade, International Mechanical Engineering Congress and Exposition, San Diego, California, USA, 2013.
- [34] A. Ammouri, H. Achdjan, A. Dorbane, G. Ayoub, G. Kridli, R. Hamade, International Mechanical Engineering Congress and Exposition, Montreal, Canada, 2014.
- [35] ASTM E3-11, Standard Guide for Preparation of Metallographic Specimens, ASTM International, West Conshohocken, PA, 2011 <http://www.astm.org>.
- [36] W.Y. Li, J.F. Li, Z.H. Zhang, D.L. Gao, Y.J. Chao, *ExM* 53 (2013) 1573–1582.
- [37] R.S. Mishra, Z.Y. Ma, *Mater. Sci. Eng. R* 50 (2005) 1–78.
- [38] J. Yang, D. Wang, B.L. Xiao, D.R. Ni, Z.Y. Ma, *MMTA* 44 (2012) 517–530.
- [39] A.N. Albakri, B. Mansoor, H. Nassar, M.K. Khraisheh, J. Mater. Process. Technol. 213 (2013) 279–290.
- [40] A.K. Rodriguez, G. Kridli, G. Ayoub, H. Zbib, *JMEP* 22 (2013) 3115–3125.
- [41] W.B. Lee, Y.M. Yeon, S.B. Jung, *Mater. Sci. Technol.* 19 (2003) 785–790.
- [42] W. Woo, H. Choo, *Sci. Technol. Weld. Join.* 16 (2011) 267–272.
- [43] ASTM E8/E8M-15a, Standard Test Methods for Tension Testing of Metallic Materials, ASTM International, West Conshohocken, PA, 2015 <http://www.astm.org>.
- [44] J. Yang, B.L. Xiao, D. Wang, Z.Y. Ma, *Mater. Sci. Eng. A* 527 (2010) 708–714.
- [45] B. Kondori, A.A. Benzerga, *MMTA* 45 (2014) 3292–3307.